Received: 27 November 2024 | Revised: 17 March 2025 | Accepted: 18 March 2025

DOI: 10.1002/cac2.70024

CANCER COMMUNICATIONS Open Access

ORIGINAL ARTICLE

Enhancing antitumor immunity through the combination of cholesterolized TLR7 agonist liposomes and radiotherapy: a role for IL-1β and the inflammasome pathway

Xuejiao Han | **Yuan Cheng** | **Dandan Wan** | **Aqu Alu** | **Ziqi Zhang** | **Zhenfei Bi** | **Manni Wang** | **Yan Tang** | **Weiqi Hong** | **Siyuan Chen** | **Li Chen** | **Yuquan Wei**

Laboratory of Aging Research and Cancer Drug Target, State Key Laboratory of Biotherapy and Cancer Center, National Clinical Research Center for Geriatrics, West China Hospital, Sichuan University, Chengdu, Sichuan, P. R. China

Correspondence
Yuquan Wei, Laboratory of Aging Research and Cancer Drug Target, State Key Laboratory of Biotherapy and Cancer Center, National Clinical Research Center for Geriatrics, West China Hospital, Sichuan University, Chengdu, Sichuan, P. R. China.
Email: yuquanwei@scu.edu.cn

Funding information
National Science Foundation for Excellent Young Scholars, Grant/Award Number: 32122052; National Natural Science Foundation Regional Innovation and Development, Grant/Award Number: U19A2003; National Natural Science Foundation of China, Grant/Award Number: 82102896; China Postdoctoral Science Foundation, Grant/Award Number: 2024M762248; Natural Science Foundation of Sichuan Province, Grant/Award Number: 2024NSFSC1883;

Abstract

Background: Radiotherapy (RT) is a key treatment modality in cancer therapy, utilizing high-energy radiation to directly kill tumor cells. Recent research has increasingly highlighted RT's potential to indirectly enhance antitumor immunity. However, this immune activation alone often fails to generate sustained systemic antitumor responses. In this study, we aimed to investigate the antitumor effects of combining cholesterolized toll-like receptor 7 (TLR7) agonist liposomes, specifically 1V209-Cho-Lip, with RT.

Methods: Mouse tumor models were used to assess the impact of combining 1V209-Cho-Lip with RT on tumor progression and modification of the tumor microenvironment. In vitro, primary mouse bone marrow-derived dendritic cells (BMDCs) were utilized to investigate changes in function and the activated pathways through RNA sequencing. Additionally, we explored the role of oxidized mitochondrial DNA (ox-mtDNA) released from irradiated tumor cells as a damage-associated molecular pattern in modulating immune responses. The involvement of interleukin-1β (IL-1β) and the inflammasome pathway in the

List of abbreviations: 8-OHdG, 8-hydroxy-2'-deoxyguanosine; ATP, adenosine triphosphate; BMDC, bone marrow-derived dendritic cell; caspase1, cysteinyl aspartate specific proteinase 1; CBA, cytometric bead array; CFSE, carboxyfluorescein succinimidyl ester; CRT, calreticulin; DAMPs, damage-associated molecular patterns; DC, dendritic cell; FBS, fetal bovine serum; FCM, flow cytometry; GO, gene ontology; H&E, hematoxylin-eosin; HMGB1, high mobility group box 1; HRP, horseradish peroxidase; i.t., intratumoral; IFN, interferon; IL, interleukin; LN, lymph node; LTS, long-term survival; MMP, mitochondrial membrane potential; nDNA, nuclear DNA; NF-κB, nuclear factor κB; NLRP3, NLR family pyrin domain containing 3; ox-mtDNA, oxidized mitochondrial DNA; PMN-MDSC, polymorphonuclear myeloid derived suppressor cell; ROS, reactive oxygen species; RT, radiotherapy; R-TCM, irradiated tumor conditioned medium; s.c., subcutaneously; SEM, standard error of mean; TLR, toll-like receptor; TNF, tumor necrosis factor; WT, wild type.

Postdoctor Research Fund of West China Hospital, Sichuan University, Grant/Award Number: 2024HXBH055

antitumor efficacy of the combined treatment was evaluated using *Il-1β*$^{-/-}$ and cysteinyl aspartate specific proteinase 1 knockout (*Casp1*$^{-/-}$) mouse models.

Results: The combination of 1V209-Cho-Lip and RT significantly inhibited tumor growth and induced antitumor immunity in tumor models. This combination therapy enhanced maturation, antigen presentation and IL-1β secretion of dendritic cells (DCs) in vitro. Ox-mtDNA released from irradiated tumor cells synergized with 1V209-Cho-Lip to activate the inflammasome pathway in DCs. The antitumor effect of the combined therapy was significantly reduced in *Il-1β*$^{-/-}$ and *Casp1*$^{-/-}$ mice.

Conclusions: This study suggests that the combination of 1V209-Cho-Lip with RT might be a promising antitumor strategy and further studies are warranted to explore the clinical relevance of this combination therapy.

KEYWORDS

cholesterolized liposome, combination therapy, IL-1β, immunotherapy, inflammasome, oxidized mitochondrial DNA, radiotherapy, TLR7 agonist

1 | BACKGROUND

Radiotherapy (RT) is an effective treatment for a range of tumors, including breast, prostate, and head and neck cancers [1]. However, cancer recurrence and metastasis can still occur following RT in clinical practice. The primary mechanism of RT involves inducing DNA double-strand breaks, which results in the release of tumor-associated antigens and various damage-associated molecular patterns (DAMPs), potentially triggering antitumor immune responses [2–4]. The abscopal effect, marked by tumor regression outside the irradiated area, suggests the activation of systemic antitumor immunity [5]. Unfortunately, this effect is notably rare in clinical settings, indicating that RT alone often fails to generate clinically significant systemic antitumor immunity in most patients. To address this, combining RT with immunostimulatory agents has been proposed as a strategy to enhance the immunogenic response, increase tumor sensitivity, and potentially reduce the required radiation dose for therapeutic efficacy. Encouragingly, numerous preclinical and clinical studies have explored these combinations, revealing promising results [6–10].

Toll-like receptors (TLRs) are highly conserved pattern recognition receptors that detect pathogen-associated molecular patterns on invading pathogens, as well as DAMPs released from damaged or dying cells [11]. These receptors are predominantly expressed on immune cells, including dendritic cells (DCs), macrophages, natural killer cells, and effector B/T cells, as well as nonimmune cells such as epithelial cells [12–14]. The majority of TLRs can activate innate defense systems and regulate downstream adaptive immune responses through the nuclear factor κB (NF-κB) and mitogen-activated protein kinases signaling pathways [15]. Consequently, TLR agonists hold potential as adjuvants to enhance immune priming induced by radiation. A recent phase I/II clinical trial evaluated the combination of a TLR9 agonist with low-dose radiation in patients with untreated indolent lymphoma. The results showed that all 29 patients experienced tumor regression at the treated sites, and 24 of these patients also had tumor reduction at non-treated sites, indicating the development of a systemic immune response [16].

TLR7 is located in the endosomal membrane, where it detects viral single-stranded RNA rich in guanosine and/or uridine. This detection triggers strong Th1-biased immune responses that promote the activation and expansion of $CD8^+$ T cells [17, 18]. However, the clinical application of TLR7 agonists is constrained by the risk of uncontrollable systemic inflammatory responses [6, 19]. To date, only imiquimod has received approval from the Food and Drug Administration for the treatment of basal cell carcinoma and other dermatologic malignancies [20]. Recently, our laboratory synthesized cholesterolized TLR7 agonist liposomes (1V209-Cho-Lip), which exhibited improved lymph node (LN) transport and fewer adverse effects compared to the TLR7 agonist 1V209 alone [21]. Furthermore, 1V209-Cho-Lip effectively induced DCs activation and elicited $CD8^+$ T cell responses. However, its efficacy was limited when used alone in the 4T1 subcutaneous tumor model.

Given the inherent immunostimulatory properties of 1V209-Cho-Lip and the in situ vaccine effect of RT, combining these two approaches may offer a promising strategy

for treating malignant tumors. Therefore, this study aims to investigate the antitumor efficacy and mechanisms of 1V209-Cho-Lip combined with RT using 4T1 and B16-F10 tumor models.

2 | MATERIALS AND METHODS

2.1 | Cell lines and reagents

Tumor cell lines B16-F10 and 4T1 were obtained from American Type Culture Collection (ATCC, Manassas, VA, USA). B16-F10 and B16-OVA cells (OVA-transfected B16-F10 cells) were cultured in DMEM medium (Gibco, Carlsbad, CA, USA), and 4T1 was cultured in RPMI 1640 (Gibco, Carlsbad, CA, USA) supplemented with 10% fetal bovine serum (FBS; Gibco, Carlsbad, CA, USA), penicillin (100 U/mL), and streptomycin (100 μg/mL) (Pen Strep; Gibco, Carlsbad, CA, USA). G418 (0.4 mg/mL) was added to the B16-OVA culture. All cell lines were maintained at 37°C in a humidified incubator with 5% CO_2. 1V209-Cho-Lip was synthesized and prepared as described previously [21]. In brief, cholesterol (1 eq), EDCI (2 eq), and DMAP (0.1 eq) were dissolved in DCM (10 mL), followed by Boc-GABA (1.2 eq). After 24 h at room temperature, the reaction mixture was extracted, washed, dried, concentrated, and purified by silica gel chromatography to yield product 1. Product 1 was then treated with 10% TFA in DCM, stirred for 1 h, extracted, dried, and concentrated to obtain product 2. Finally, 1V209 (1 eq), HATU (1.2 eq), and TEA (2 eq) were dissolved in DMF, and product 2 (1.2 eq) was added dropwise. After 48 h, DMF was removed, and the residue was purified to yield 1V209-Cho. 1V209-Cho-Lip was prepared by thin film hydration. SPC, cholesterol, and 1V209-Cho (65:32:3 molar ratio) were dissolved in chloroform/methanol (10:1), evaporated to form a lipid film at 37°C, and hydrated in PBS for 1 h. The solution was sonicated in water for 30 min, then probe-sonicated at 80W for 120 s.

2.2 | Mice

The BALB/C mice (female, 6-8 weeks) and C57BL/6 mice (female, 6-8 weeks, 18-20 g) were purchased from Vital River (Beijing, China). Cysteinyl aspartate specific proteinase 1 knockout (*Casp1*$^{-/-}$) and NLR family pyrin domain containing 3 knockout (*Nlrp3*$^{-/-}$) mice were obtained from Jackson Laboratory (Bar Harbor, Maine, USA). Interleukin-1β knockout (*Il-1β*$^{-/-}$) mice were from Tokyo University of Science (Tokyo, Japan). All mice were housed in specific-pathogen-free facilities under consistent room temperature and humidity. The animal study was approved by the Institutional Animal Care and Use Committee of Sichuan University (20250108003). Mice were euthanized by cervical dislocation when body weight loss exceeded 20%, tumor burden surpassed 10% of body weight, or a significant decline in mobility was observed.

2.3 | Tumor challenge and treatments

For mice bearing a single tumor, 1×10^5 4T1 or 5×10^5 B16-F10 cells were suspended in 100 μL of serum-free medium and subcutaneously (s.c.) injected into the right proximal hind legs of mice. For mice bearing bilateral tumors, mice were injected s.c. with 1×10^5 4T1 or 5×10^5 B16-F10 cells in the right proximal hind legs (primary tumor); 2 days later, 5×10^4 4T1 or 2×10^5 B16-F10 cells were implanted in the left hind legs (secondary tumor).When tumors reached a volume of approximately 50 mm^3 (10 days after injection), the mice were randomly divided into 5 groups, with 6-8 mice in each group. Mice from RT alone and combination therapy (RT + 1V209-Cho-Lip) groups received local radiation using an X-ray generator (XCELL320, KUBTEC, Milford, CT, USA) at a dose rate of 2 Gy/min. Before irradiation, each mouse was anesthetized and shielded by a lead box with only the tumor exposed. Following radiation, animals from the 1V209-Cho-Lip and combined therapy groups received four intratumoral (i.t.) injections of 1V209-Cho-Lip (3 mg/kg) on days 11, 14, 17, and 20. Tumor volume and body weight were monitored every three days. Tumor volume was calculated as length × width^2 × 1/2. Mice were sacrificed on day 24 or 31 post-tumor inoculation, and the tumors were harvested, weighed, and photographed. For the 4T1 tumor, the presence of metastases in the lungs was assessed, and the lungs were harvested and photographed. The number of metastatic nodules in the lungs was counted. The survival time of mice was recorded from the date of tumor inoculation to the date of death or sacrifice when the tumor volume reached 2, 000 mm^3.

2.4 | Flow cytometry (FCM) analysis

The immune microenvironment of the tumor, metastatic lung tissue, and tumor-draining LNs was analyzed by FCM. Tumor-draining inguinal LNs were collected and triturated to obtain single-cell suspensions. Tumor and metastatic lung tissues were finely chopped and digested into single-cell suspensions using 1 mg/mL collagenase Type I (Gibco, Carlsbad, CA, USA), 0.5 mg/mL Type IV (Gibco, Carlsbad, CA, USA), and 10 μg/mL DNase I (Sigma-Aldrich, St Louis, MO, USA) in RPMI 1640 medium (Gibco, Carlsbad, CA, USA) for 1 h at 37°C. Then,

the suspensions were filtered through a 70 μm nylon mesh filter and stained with antibodies. All fluorescently labeled antibodies were purchased from BioLegend (San Diego, CA, USA), or BD Biosciences (San Jose, CA, USA), with detailed antibody information provided in Supplementary Table S1. The LIVE/DEAD™ Fixable Near-IR Dead Cell Stain Kit (L34975, Thermo Fisher Scientific, Carlsbad, CA, USA) was employed to exclude dead cells. For cell surface staining, cells were incubated with antibodies for 30 min in PBS at 4°C in the dark and subsequently washed twice with PBS. For intracellular staining, cells were fixed and permeabilized using BD Cytofix/Cytoperm™ solution (BD Biosciences, San Jose, CA, USA) according to the manufacturer's protocol. Subsequently, the cells were stained with intracellular antibodies overnight at 4°C. All samples were analyzed on a NovoCyte Flow Cytometer (ACEA Biosciences, San Diego, CA, USA) and using NovoExpress® software (1.3.0, ACEA Biosciences, San Diego, CA, USA).

2.5 | Bone marrow derived dendritic cells (BMDCs) generation

BMDCs were prepared as described in our previous study [22]. Briefly, bone marrow cells were isolated from the femurs and tibiae of C57BL/6 mice and filtered through a 70 μm nylon mesh filter. Then the cells were cultured in complete RPMI-1640 medium supplemented with 20 ng/mL granulocyte-macrophage colony stimulating factor (PeproTech, Rocky Hill, NJ, USA), 10 ng/mL IL-4 (Sigma-Aldrich, St Louis, MO, USA), 50 μmol/L β-mercaptoethanol (Sigma-Aldrich, St Louis, MO, USA), and 1 mmol/L sodium pyruvate (Gibco, Carlsbad, CA, USA) for 7 days. Fresh medium containing all growth factors was replenished on days 3 and 6. Finally, the BMDCs were harvested for subsequent experiments.

2.6 | Preparation of irradiated tumor conditioned medium (R-TCM)

Tumor cells that were plated into 10 cm cell culture dishes were irradiated with a single dose of 16 Gy by an X-ray generator (XCELL320, KUBTEC, Milford, CT, USA, 2 Gy/min). The medium was then replaced with 10 mL of serum-free medium. After 48 h, the medium was collected and centrifuged at 4000 × g for 30 min to remove tumor cells and debris. Then, the supernatant was filtered through a 0.22 μm Millipore microporous membrane (Merck Millipore, Burlington, MA, USA) and stored at -20°C until further use.

2.7 | Detection of cytokines

The concentrations of tumor necrosis factor (TNF)-α, IL-6, IL-12, IL-1β and interferon (IFN)-γ in the culture supernatants were determined using a BD™ Cytometric Bead Array (CBA) (558266; BD Biosciences, San Jose, CA, USA), following the manufacturer's guidelines. Briefly, the samples and standards were initially mixed with capture beads and incubated for 1 h at room temperature. Subsequently, the PE detection reagent was added to each assay tube, and the mixture was incubated for an additional 1 h at ambient temperature. After washing with wash buffer, the samples were analyzed by FCM and the data were processed using FCAP Array V3.0 (BD Biosciences, San Jose, CA, USA).

2.8 | T cell proliferation and activation assay

To investigate the antigen cross-presentation, the $CD8^+$ T cell proliferation and activation assay were performed. BMDCs derived from wild-type (WT) mice were cultured for 7 days and then stimulated with 1V209-Cho-Lip (10 μg/mL), R-TCM (10%) or both for 24 h. Then, the cells were collected and resuspended in RPMI 1640 for further experiments.

Simultaneously, splenic lymphocytes were isolated from mice on day 14 pre-inoculated with B16-OVA, and then labelled with carboxyfluorescein succinimidyl ester (CFSE) (C34554, Invitrogen, Carlsbad, CA, USA) by incubation with 2.5 μmol/L CFSE for 15 min in the dark at 37°C. Subsequently, serum-containing medium was added and incubated for 5 min. After washing, the labelled lymphocytes were cocultured with treated BMDCs at a 5:1 ratio, and then OVA peptide (10 μg/mL) was added to cells following by 48 h of incubation at 37°C. Images of lymphocytes were captured using an inverted light microscope, and the cells were collected for flow cytometric analysis to measure CFSE fluorescence intensity in T cells. To detect the activation of OVA-specific cytotoxic T cells, the cells were collected and labeled with T-select MHC Tetramer/H-2Kb-OVA (SIINFEKL) (TS-5001-1C, MBL, Tokyo, Japan) for flow cytometric analysis. Additionally, the culture supernatants were collected to quantify cytokine concentrations.

2.9 | RNA sequencing and bioinformatics analysis

BMDCs were treated with R-TCM (10%) and 1V209-Cho-Lip (10 μg/mL) for 48 h, and then lysed with TRIzol

(Invitrogen, Carlsbad, CA, USA). The filtered reads were mapped to the reference genome using HISAT2 (v 2.1.0). We used HTSeq (v 0.9.1) statistics to compare the Read Count values on each gene, and then used FPKM to standardize the expression. Differential gene expression analysis was conducted using DESeq (v1.38.3) with the following screening criteria: |log2 (fold change)| > 1 and significant P value < 0.05. Then R package clusterProfiler was used to perform gene ontology (GO) functional enrichment analysis of differential genes.

2.10 | Detection of cell apoptosis, mitochondrial membrane potential (MMP) and reactive oxygen species (ROS)

Tumor cells were seeded in 12-well plates and exposed to 8 Gy, 16 Gy, or 32 Gy radiation using an X-ray generator (XCELL320, KUBTEC, Milford, CT, USA, 2 Gy/min), with a non-irradiated group serving as the control. After incubation for 48 h, apoptotic cells were detected by the FITC AnnexinV-Apoptosis Detection Kit from BD Pharmingen (San Jose, CA, USA). And the cells were stained with 2.5 μmol/L JC-1 (5,5,6,6-tetrachloro-1,1,3,3-tetraethylbenzimidazolylcarbocyanine iodide) (Thermo Fisher Scientific, Carlsbad, CA, USA) for 15 min at room temperature or 10 μmol/L H2DCFDA (2',7'-dichlorofluorescein diacetate) (Invitrogen, Carlsbad, CA, USA) for 30 min at 37°C in the dark. Subsequently, the samples were washed three times with PBS and analyzed by FCM.

2.11 | Detection of intracellular 8-OHdG (8-hydroxy-2'-deoxyguanosine) content

Tumor cells were incubated for 30 h following exposure to 16 Gy X-ray radiation. Then, the cells were harvested and incubated with a goat anti-8-OHdG antibody (10802, Abcam, Cambridge, MA, USA) at 4°C overnight following fixation and permeabilization. The next day, cells were stained with a FITC-conjugated donkey anti-goat IgG antibody (1:1000; #ab6881; Abcam, Cambridge, MA, USA) for 1 h at 4°C, and analyzed via FCM.

2.12 | Immunohistochemistry and hematoxylin-eosin (H&E) staining

Tissues obtained from mice were fixed in 4% paraformaldehyde and embedded in paraffin. The sections were deparaffinized in xylene and rehydrated through graded ethanol concentrations. Endogenous peroxidase activity was then blocked, and antigen retrieval was performed. After blocking nonspecific binding sites with goat serum, the sections were incubated with primary antibodies. The slides were subsequently treated with horseradish peroxidase (HRP)-conjugated secondary antibodies and a streptavidin-biotin complex. HRP activity was visualized using a diaminobenzidine peroxide solution, and cell nuclei were counterstained with hematoxylin. All the reagents used were purchased from Beyotime Institute of Biotechnology (Shanghai, China). For H&E staining, the tissue sections were rehydrated and stained using an H&E Staining Kit (Solarbio, Beijing, China). The data were visualized with the Pannoramic MIDI II system (3DHISTECH Ltd., Budapest, Hungary) and analyzed with Case Viewer software (3DHISTECH Ltd., Budapest, Hungary).

2.13 | Immunofluorescence staining

The cells were seeded on poly-L-ornithine -coated coverslips (Sigma-Aldrich, St Louis, MO, USA) in 24-well plates. After treatment, the cells were fixed in 4% paraformaldehyde and permeabilized with 0.2% Triton X-100 in PBS for 10 min at room temperature. The cells were then blocked with 2% goat serum for 30 min at room temperature and incubated with primary antibodies overnight at 4°C. The next day, cells underwent incubation with secondary antibodies for 1 h in darkness at room temperature, followed by three washes with PBS. Finally, the coverslips were mounted with Prolong Gold antifade reagent containing DAPI (Life Technologies, Carlsbad, CA, USA), and the cells were observed using Olympus FV1000 confocal microscopy (Olympus, Tokyo, Japan). A detailed list of the antibodies used is provided in Supplementary Table S1.

2.14 | Mitochondrial DNA isolation and transfection

Purified mtDNA was isolated from irradiated tumor cells using the mtDNA Isolation Kit (#ab65321; Abcam, Cambridge, MA, USA), following the manufacturer's protocol. This was followed by phenol-chloroform extraction and isopropanol precipitation to eliminate cellular proteins. After incubation with LPS (500 ng/mL) for 3 h, BMDCs were transfected with the isolated mtDNA using Lipofectamine™ 3000 (Invitrogen, Carlsbad, CA, USA), as described previously [23].

2.15 | Immunoblotting

BMDCs were stimulated with the indicated treatment at various time points. Supernatants were subsequently

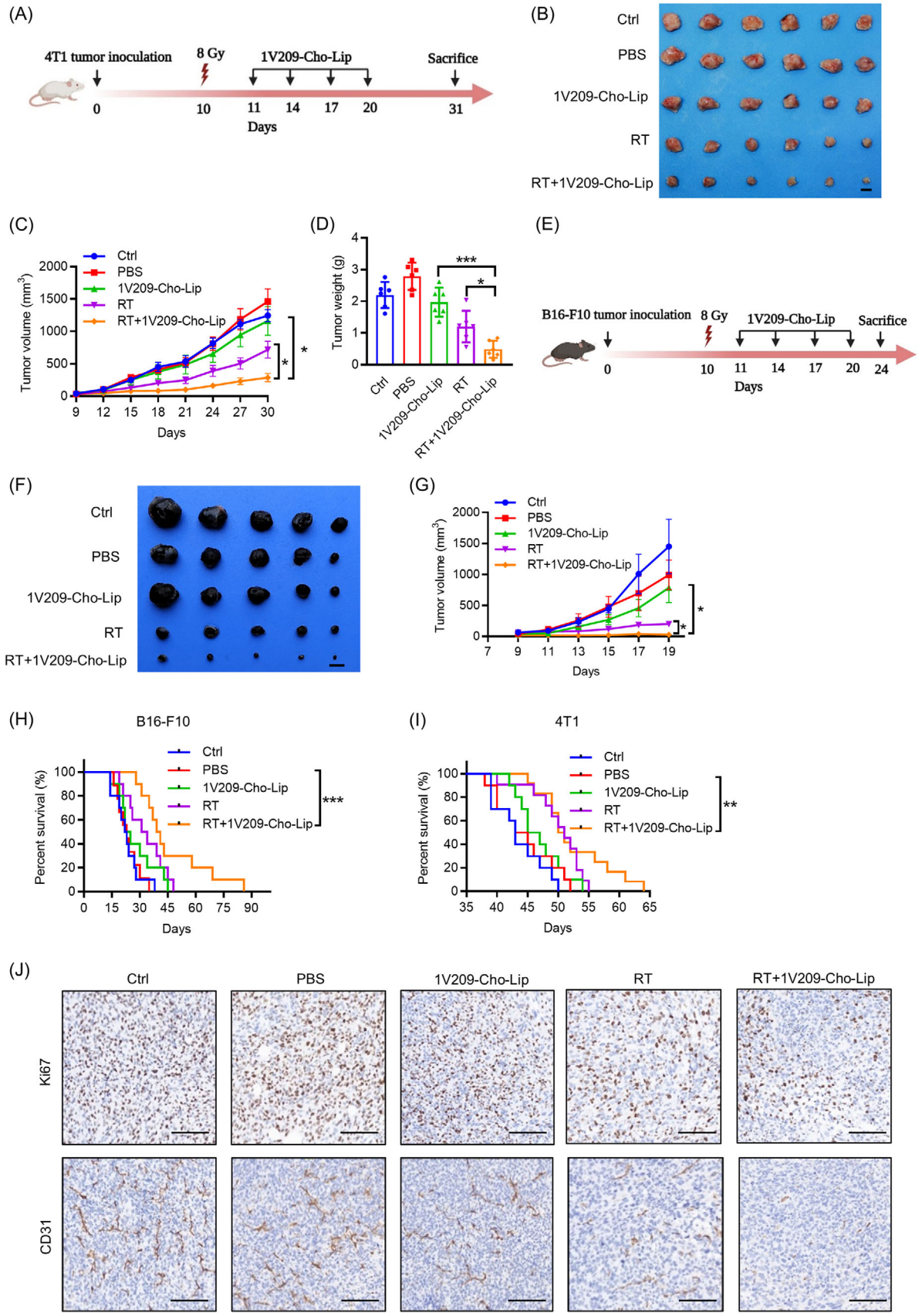

FIGURE 1 Combining 1V209-Cho-Lip with RT effectively inhibited primary tumor growth and prolonged survival in 4T1 and B16-F10 tumor models. (A) Schematic diagram of treatment protocol in the 4T1 subcutaneous tumor model. Mice were administered a single 8 Gy local radiation dose on day 10, followed by four i.t. injections of 1V209-Cho-Lip (3 mg/kg) on days 11, 14, 17, and 20. (B) Representative images of resected tumors from different groups in the 4T1 tumor model ($n = 6$ per group). Bar = 10 mm. (C) Tumor growth curve of 4T1 tumors

collected and concentrated using the trichloroacetic acid/acetone precipitation method [24]. Cells were lysed in RIPA lysis buffer (Beyotime, Shanghai, China) containing a proteinase inhibitor cocktail (Sigma-Aldrich, St Louis, MO, USA) and a phosphatase inhibitor cocktail (KeyGen, Jiangsu, China). Protein concentrations were measured using the BCA (Bicinchoninic Acid Assay) Protein Assay (Pierce, Thermo Fisher Scientific, Carlsbad, CA, USA). Equal amounts of proteins were separated by SDS-PAGE gels and transferred onto Millipore PVDF (poly vinylidene fluoride) membranes (Merck Millipore). Membranes were blocked with 5% milk dissolved in TBS-T for 1 h at room temperature, followed by an overnight incubation at 4°C with antibodies against p-IκBα (Ser32), total IκBα, p-p65 (Ser536), total p65, GAPDH, and caspase-1 (detailed information is provided in Supplementary Table S1). Subsequent incubation with the appropriate secondary HRP-conjugated antibodies, bands were detected using Immobilon™ Western Chemiluminescent HRP Substrate (Millipore) and ChemiDoc MP imaging system (Bio-Rad Laboratories). Band intensity was analyzed by Image J 2.1.0 (Java. NIH, USA).

2.16 | Quantitative real-time polymerase chain reaction (qRT-PCR)

Total cellular RNA was extracted using an isolation kit (Foregene, Chengdu, China) and reversely transcribed into cDNA with a reverse transcription kit (Takara Bio, Tokyo, Japan) according to the manufacturer's instructions. Then, qRT-PCR was performed with SYBR Green Real-Time PCR master mixes (Qiagen, Germany) with Bio-Rad CFX96 using a two-step PCR protocol. The relative gene expression was calculated by the $2^{-\Delta\Delta Ct}$ method using *Gapdh* as a house-keeping gene. The primers used are shown below: the forward primer 5'-AGGAGCTATCACTTGACCACATCT-3' and the reverse primer 5'-GCGAGATTTGAAGCTGGATGC-3' for *Il-1β*; the forward primer 5'-AGAAAGCCGCCTCAAACCTT-3' and the reverse primer 5'- GCGGTTGTACAGTGAAGTCG-3' for *Il-18* and the forward primer 5'-ACCCAGAAGACTGTGGATGG-3' and the reverse primer 5'- ACATTGGGGGTAGGAACAC-3' for *Gapdh*.

2.17 | Statistical analysis

The data were analyzed using GraphPad Prism 9 software (GraphPad Prism, San Diego, CA, USA), and are presented as means ± standard error of mean (SEM). Comparisons between two groups were conducted via a two-tailed unpaired Student's *t*-test, while multiple groups were analyzed utilizing one-way or two-way analysis of variance (ANOVA). Survival data were assessed by the log-rank (Mantel-Cox) test. For all tests, statistical significance was defined as $P < 0.05$.

3 | RESULTS

3.1 | 1V209-Cho-Lip synergized with local RT to inhibit primary tumor growth and prolong survival

To evaluate the antitumor therapeutic effect of 1V209-Cho-Lip combined with RT, two subcutaneous tumor models, 4T1 (murine mammary carcinoma) and B16-F10 (melanoma), were employed. Tumor-bearing mice were administered a single 8 Gy dose of local radiation on day 10, when the tumors were approximately 50 mm^3, followed by four i.t. injections of either PBS or 1V209-Cho-Lip (3 mg/kg) on days 11, 14, 17, and 20 (Figure 1A). As previously reported [21], 1V209-Cho-Lip monotherapy showed no therapeutic effect in the subcutaneous 4T1 model compared to PBS treatment (Figure 1B-D). However, the combination of 1V209-Cho-Lip with RT significantly inhibited the growth of 4T1 tumors compared to either 1V209-Cho-Lip alone or RT monotherapy (Figure 1B-D). Similarly, the combination of 1V209-Cho-Lip and RT demonstrated the highest antitumor efficacy in the B16-F10 mouse model compared to the other treatment

($n = 6$ per group), showing significant inhibition of tumor growth in the RT + 1V209-Cho-Lip group compared to monotherapy or control groups. (D) Average weight of resected tumors in the 4T1 tumor model ($n = 6$ per group). (E) Schematic diagram of treatment protocol in the B16-F10 subcutaneous tumor model. Mice were administered a single 8 Gy local radiation dose on day 10, followed by four i.t. injections of 1V209-Cho-Lip (3 mg/kg) on days 11, 14, 17, and 20. (F) Representative images of resected tumors from different groups in the B16-F10 tumor model ($n = 5$ per group). Bar = 10 mm. (G) Tumor growth curve of B16-F10 tumors ($n = 5$ per group), indicating the highest antitumor efficacy in the combination therapy group. (H-I) Survival curves of mice bearing B16-F10 (H) and 4T1 (I) tumors treated with RT + 1V209-Cho-Lip ($n = 10$-12 per group). The combination therapy significantly improved survival compared to other groups. (J) Immunohistochemical staining of Ki67 and CD31 in paraffin-embedded 4T1 tumor sections demonstrated that RT + 1V209-Cho-Lip reduced proliferation (Ki67) and microvessel density (CD31). Bar = 100 μm. Data are presented as means ± SEM. Statistical analyses were performed using one-way ANOVA (D) and two-way ANOVA (C and G). Survival data were analyzed with the log-rank (Mantel-Cox) test (H and I). *$P < 0.05$; **$P < 0.01$; ***$P < 0.001$. Abbreviations: Gy, gray; i.t., intratumoral; RT, radiotherapy.

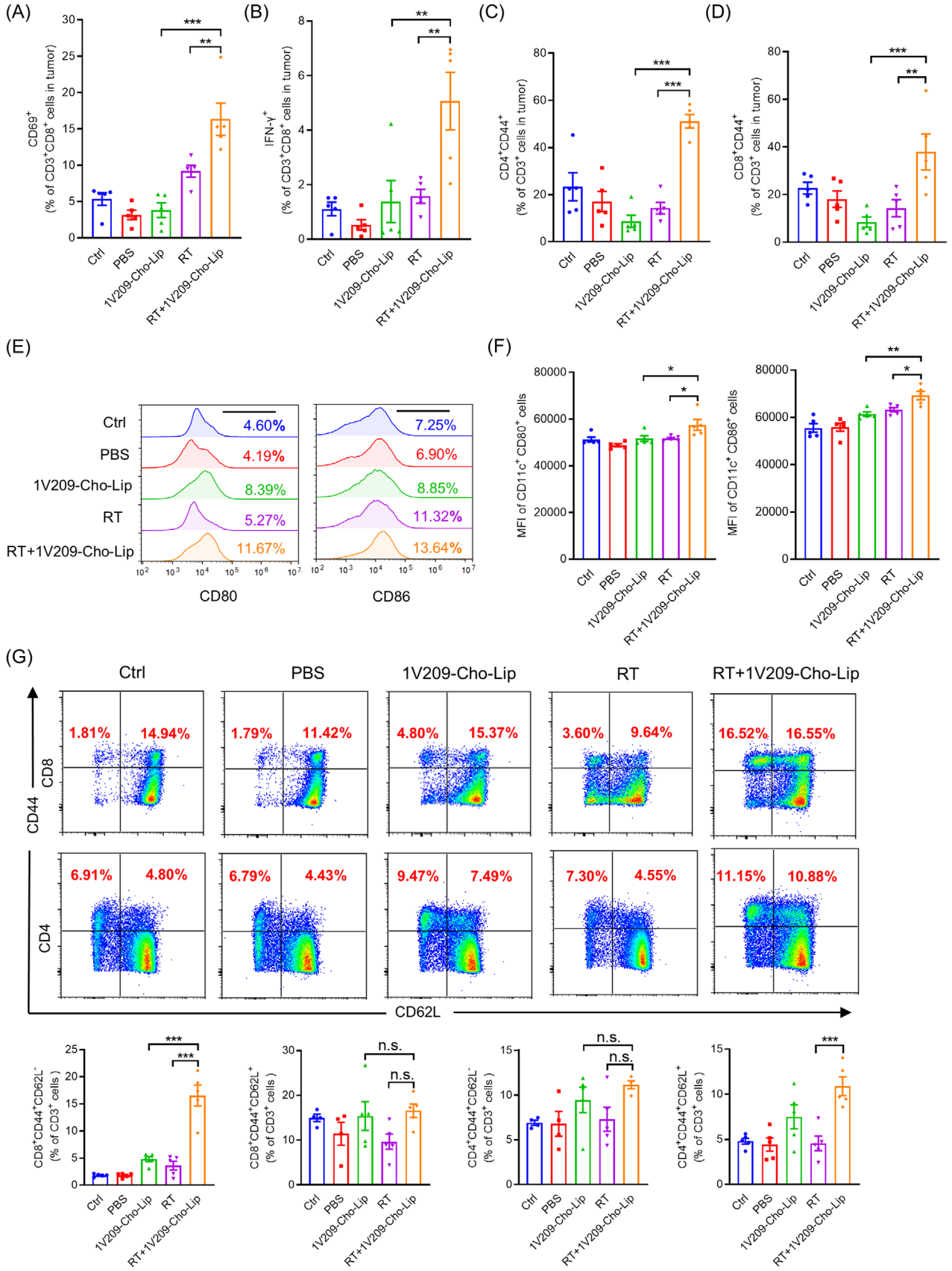

FIGURE 2 1V209-Cho-Lip combined with RT induced effective antitumor immunity in both tumor tissues and tumor-draining LNs. (A-B) FCM analysis revealed that the combination therapy significantly increased the proportions of active $CD8^+$ T cells ($CD3^+CD8^+CD69^+$ and $CD3^+CD8^+IFN\text{-}\gamma^+$) within the tumor compared to other treatment groups ($n = 5$ per group). (C-D) $CD4^+$ memory T cells

groups (Figure 1E-G). Consistently, the combination therapy was associated with improved mouse survival compared with monotherapy. Median survival time was significantly extended in B16-F10 mice treated with RT + 1V209-Cho-Lip, with values of 23.0 days for PBS, 23.5 days for 1V209-Cho-Lip, 32.5 days for RT, and 40.0 days for RT + 1V209-Cho-Lip (Figure 1H). Furthermore, RT + 1V209-Cho-Lip significantly enhanced long-term survival (LTS, defined as survival more than 55 days after treatment) in mice bearing 4T1 tumors. Approximately 33% (4/12) of mice in the combination group achieved LTS, compared to none in the other groups (Figure 1I). We subsequently conducted immunohistochemical analyses of 4T1 tumor tissues. As illustrated in Figure 1J, the RT + 1V209-Cho-Lip treatment significantly reduced both the number of Ki67-positive cells and the microvessel density (measured by CD31 staining) compared to the other groups. However, mice treated with RT + 1V209-Cho-Lip did not inhibit secondary tumor growth in 4T1 or B16-F10 tumor models (Supplementary Figure S1A-D). Studies have demonstrated the superiority of fractionated RT in inducing antitumor immunity compared with a single large dose of radiation [25]. Therefore, we administered a fractionated regimen of 2 Gy × 4 fractions in mice bearing 4T1 tumors. However, no significant difference in tumor growth inhibition was observed between the combination therapy and fractionated RT alone (Supplementary Figure S1E-G). This outcome may partly be attributed to immune exhaustion or tolerance induced by the fractionated RT.

3.2 | 1V209-Cho-Lip in combination with RT induced effective antitumor immunity in both tumor tissues and tumor-draining LNs

We investigated whether RT combined with 1V209-Cho-Lip could stimulate antitumor immunity in primary tumors and tumor-draining inguinal LNs. We found that activated $CD8^+$ T cells ($CD3^+CD8^+CD69^+$), effector $CD8^+$ T cells ($CD3^+CD8^+$ IFN-γ^+), memory $CD4^+$ T cells ($CD3^+CD4^+CD44^+$) and memory $CD8^+$ T cells ($CD3^+CD8^+CD44^+$) were significantly increased in the combination therapy group compared to the RT or 1V209-Cho-Lip monotherapy groups (Figure 2A-D and Supplementary Figure S2). DCs are specialized antigen-presenting cells predominantly located in LNs. Therefore, we assessed whether the combined treatment could enhance DCs maturation in the inguinal LNs. As shown in Figure 2E-F, the RT + 1V209-Cho-Lip treatment effectively activated DCs, as evidenced by the upregulation of maturation markers CD80 and CD86. Furthermore, this combination therapy significantly increased the percentages of both $CD8^+$ effector memory T cells ($CD8^+CD44^+CD62L^-$) and $CD4^+$ central memory T cells ($CD4^+CD44^+CD62L^+$) in the draining inguinal LNs, outperforming the monotherapy groups (Figure 2G). Although there was an increasing trend in $CD8^+$ central memory T cells ($CD8^+CD44^+CD62L^+$) and $CD4^+$ effector memory T cells ($CD4^+CD44^+CD62L^-$), no statistically significant difference was observed between the combination therapy and monotherapy (Figure 2G). Additionally, we found that 1V209-Cho-Lip monotherapy group and the combination therapy group exhibited reduced spontaneous metastatic nodules and lower percentages of polymorphonuclear myeloid derived suppressor cells (PMN-MDSCs) ($Ly6G^+Ly6C^{int}$) in the lungs of 4T1 tumor model when compared to other groups (Supplementary Figure S3).

3.3 | The combination of 1V209-Cho-Lip and R-TCM enhanced DCs maturation and antigen presentation in vitro

We further investigated the effects of RT combined with 1V209-Cho-Lip in DCs in vitro. To simulate the tumor RT microenvironment in vitro, we employed a conditioned medium comprising 10% R-TCM along with 1V209-Cho-Lip (10 μg/mL) to stimulate primary mouse BMDCs. Our findings revealed a significant increase in the mean fluorescence intensity (MFI) of costimulatory molecules, including CD80 and CD86, on the surface of DCs in the combination group compared to the other groups (Figure 3A-B). Additionally, levels of cytokines such as TNF-α, IL-1β, and IL-12 were also markedly elevated following combination stimulation. However, the secretion of IL-6 in the combination therapy group did not

($CD3^+CD4^+CD44^+$) and $CD8^+$ memory T cells ($CD3^+CD8^+CD44^+$) were significantly elevated in the tumor microenvironment following combination therapy ($n = 5$ per group). (E) Representative histograms of FCM showed enhanced expression of CD80 and CD86 on DCs in tumor-draining LNs after combination treatment. (F) Quantification of MFI value of $CD11c^+CD80^+$ and $CD11c^+CD86^+$ cells in tumor-draining LNs ($n = 5$ per group). (G) Illustrative FCM plots and quantification of effector memory T cells ($CD8^+CD44^+CD62L^-$) and central memory T cells ($CD4^+CD44^+CD62L^+$) in tumor-draining LNs ($n = 4$-5 per group). Data are expressed as means ± SEM and analyzed using one-way ANOVA. $^*P < 0.05$; $^{**}P < 0.01$; $^{***}P < 0.001$; n.s., not significant. Abbreviations: FCM, flow cytometry; LN, lymph node; MFI, mean fluorescence intensity; RT, radiotherapy.

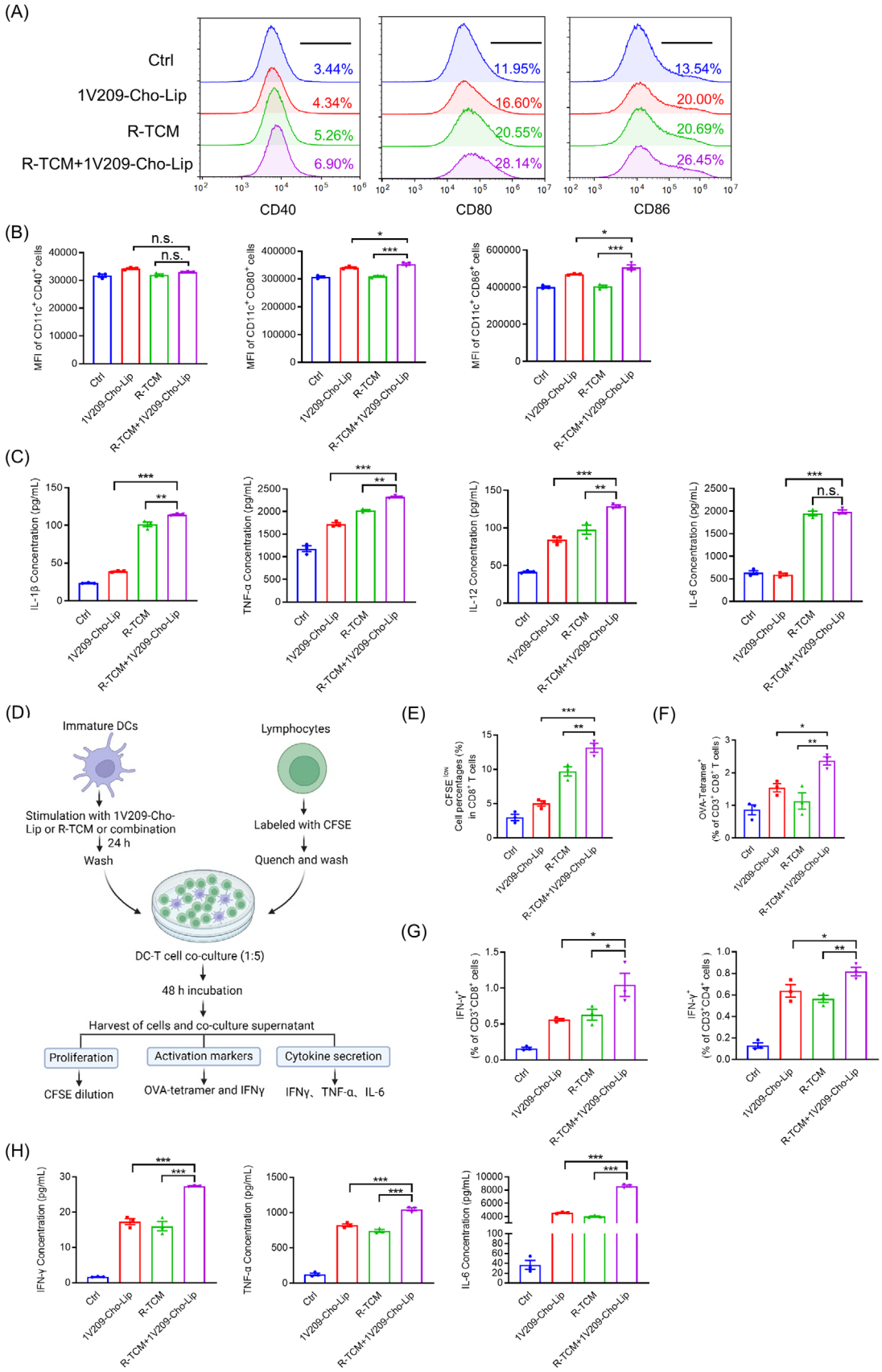

FIGURE 3 The combination of 1V209-Cho-Lip and R-TCM enhanced DCs maturation and antigen presentation in vitro. (A) Representative histograms of FCM showed the expression of CD40, CD80, and CD86 on DCs following stimulation with 1V209-Cho-Lip (10 μg/mL) and R-TCM (10%). (B) Quantification of MFI value of $CD11c^+CD40^+$, $CD11c^+CD80^+$, and $CD11c^+CD86^+$ cells following stimulation

differ from that in the radiotherapy group (Figure 3C). To evaluate the antigen presentation capability of BMDCs post-stimulation, they were cocultured with CFSE-labeled splenic lymphocytes derived from B16-OVA-inoculated mice (Figure 3D). FCM analysis revealed significantly increased CFSE fluorescence dilution which indicated 1V209-Cho-Lip combined with R-TCM could significantly contribute to the antigen presentation and the proliferation of $CD8^+$ T cells (Figure 3E and Supplementary Figure S4A-B). To further explore whether 1V209-Cho-Lip + R-TCM could induce antigen-specific cell-mediated adaptive immunity, T cells were collected and labeled with SIINFEKL and antibodies for FCM analysis. FCM analysis indicated a higher percentage of OVA-specific $CD8^+$ T cells (Figure 3F and Supplementary Figure S4C) and IFN-γ production in both $CD4^+$ and $CD8^+$ T cells in the combination group compared to the other groups (Figure 3G and Supplementary Figure S4D). Furthermore, cytokines secreted by activated T cells, including IFN-γ, TNF-α, and IL-6, were significantly increased after combination stimulation (Figure 3H). These results suggest that the combination of 1V209-Cho-Lip and R-TCM effectively promotes DC maturation and enhances their antigen presentation capabilities, leading to the proliferation and activation of T cells.

3.4 | The combination of 1V209-Cho-Lip and R-TCM enhanced IL-1β secretion

To investigate the underlying mechanisms, we employed high-throughput sequencing to identify transcriptome changes in DCs following treatment with 1V209-Cho-Lip (10 μg/mL) and R-TCM (10%). Analysis of the transcriptome sequencing data revealed that IL-1β was significantly up-regulated after treatment with 1V209-Cho-Lip combined with R-TCM (Figure 4A-B). GO enrichment analysis further identified that biological processes related to responses to external stimuli and immune system functions were enriched post-treatment (Figure 4C). IL-1β is activated and released through the inflammasome by caspase-1-mediated cleavage of its precursor form [26]. To determine whether 1V209-Cho-Lip and R-TCM induce IL-1β secretion via the inflammasome pathway, we stimulated BMDCs from WT, *Nlrp3*$^{-/-}$, and *Casp1*$^{-/-}$ mice with 10 μg/mL of 1V209-Cho-Lip and R-TCM for 48 h. Supernatants were collected to measure IL-1β levels, revealing impaired production in *Casp1*$^{-/-}$ BMDCs and a partial reduction in *Nlrp3*$^{-/-}$ BMDCs (Figure 4D), suggesting IL-1β is secreted through the inflammasome pathway. Additionally, immunohistochemical analyses of IL-1β in tumor tissues showed that RT + 1V209-Cho-Lip treatment significantly enhanced IL-1β secretion (Figure 4E).

3.5 | Oxidized mitochondrial DNA (ox-mtDNA) from irradiated tumor cells synergized with 1V209-Cho-Lip to activate the inflammasome pathway in DCs

RT can induce immunogenic cell death and stimulate tumor-specific immune responses by exposing and releasing various DAMPs [27]. Our laboratory previously demonstrated that cationic nanocarriers can trigger cell necrosis and mtDNA leakage, resulting in innate immune response in vivo [28]. We hypothesized that oxidized mtDNA from irradiated tumor cells may act as a DAMP to enhance antitumor immune responses. To test this hypothesis, we assessed tumor cell death and ROS generation following RT in vitro. Tumor cells were exposed to 8 Gy, 16 Gy, or 32 Gy of radiation, and after 48 h of incubation, they were analyzed using Annexin-V and PI staining. As shown in Figure 5A and Supplementary Figure S5A, the total proportion of early (Annexin V^+/PI^-) and late (Annexin V^+/PI^+) apoptotic cells markedly increased from 2.49% (Non-IR) to 13.28%, 18.13% and 18.92% in response to 8 Gy, 16 Gy and 32 Gy radiation, respectively. Similarly, radiation treatment induced ROS generation and a decrease in MMP with increasing radiation doses (Figure 5B-C and Supplementary Figure S5B-C). Based on these results, we selected 16 Gy for further investigations. ROS are highly reactive oxygen-containing molecules that can

with 1V209-Cho-Lip (10 μg/mL) and R-TCM (10%) ($n = 3$ per group). (C) Supernatants were collected from DCs following stimulation with 1V209-Cho-Lip (10 μg/mL) and R-TCM (10%) to measure levels of IL-1β, TNF-α, IL-12, and IL-6 using CBA analysis ($n = 3$ per group). (D) Schematic representation of the coculture system where BMDCs were stimulated and cocultured with CFSE-labeled T cells. (E) Quantification of percentages of $CFSE^{low}$ $CD8^+$ T cells after cocultured with BMDCs ($n = 3$ per group). (F) Quantification of percentages of the OVA-specific $CD8^+$ T cells after cocultured with BMDCs ($n = 3$ per group). (G) FCM analysis of IFN-γ production in $CD4^+$ and $CD8^+$ T cells after cocultured with BMDCs ($n = 3$ per group). (H) Levels of IFN-γ, TNF-α, and IL-6 in the supernatants were quantified via CBA ($n = 3$ per group). Data are expressed as means ± SEM and analyzed using one-way ANOVA. *$P < 0.05$; **$P < 0.01$; ***$P < 0.001$; n.s., not significant. Abbreviations: BMDC, bone marrow-derived dendritic cell; CBA, cytometric bead array; CFSE, carboxyfluorescein succinimidyl ester; DC, dendritic cell; FCM, flow cytometry; IFN, interferon; IL, interleukin; MFI, mean fluorescence intensity; OVA, ovalbumin; R-TCM, irradiated tumor conditioned medium; TNF, tumor necrosis factor.

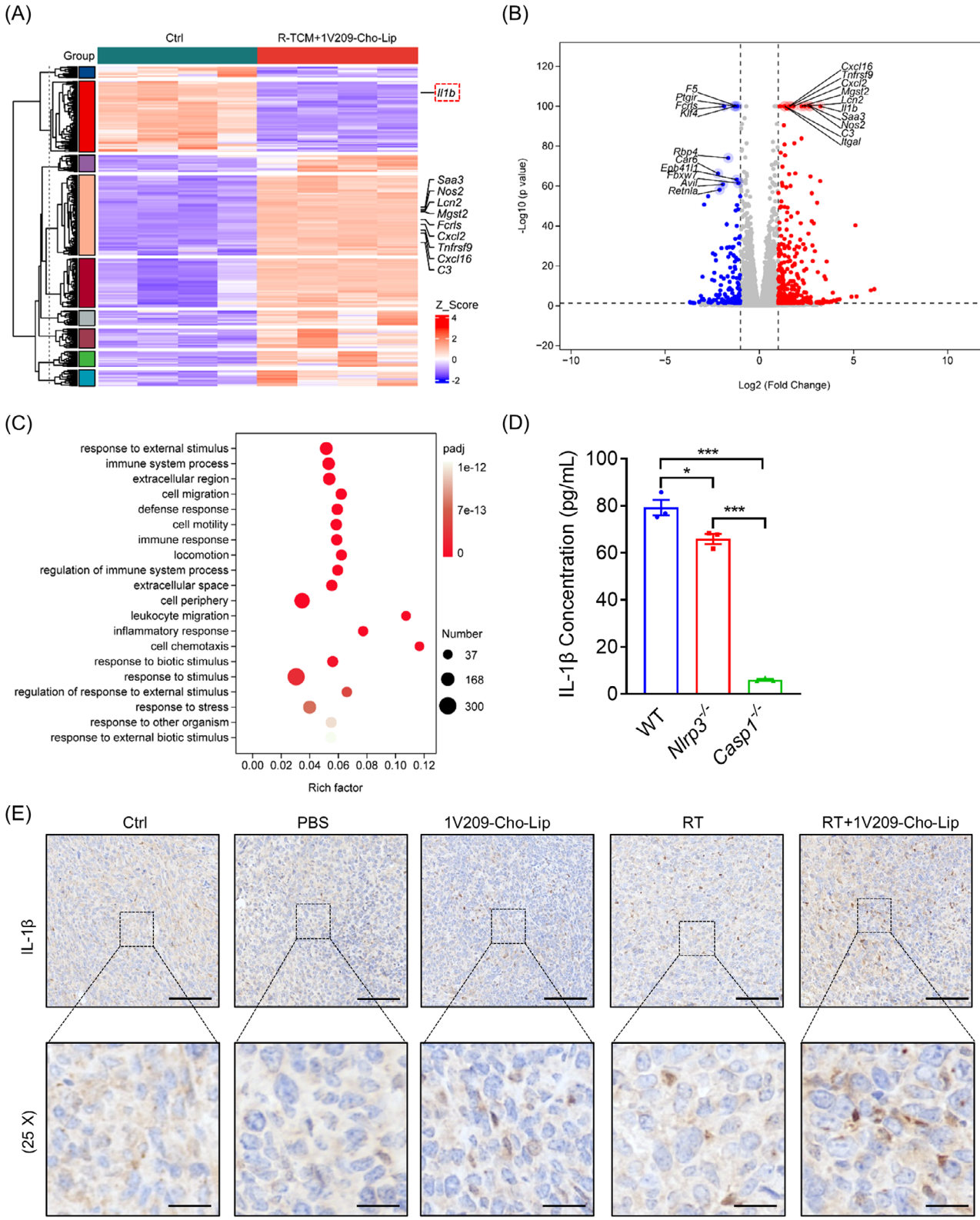

FIGURE 4 The combination of 1V209-Cho-Lip and R-TCM enhanced IL-1β secretion. (A) Heatmap displaying differential mRNA expression between control and 1V209-Cho-Lip + R-TCM groups ($n = 4$ per group). (B) Volcano plot showing the top 10 up-regulated and down-regulated mRNAs in the 1V209-Cho-Lip + R-TCM group. (C) The top 20 enriched genes in the GO biological process categories after 1V209-Cho-Lip + R-TCM treatment. (D) BMDCs from WT, *Nlrp3*$^{-/-}$, and *Casp1*$^{-/-}$ mice were stimulated with 1V209-Cho-Lip and R-TCM for 48 h; supernatants were collected to measure IL-1β levels via CBA ($n = 3$ per group). (E) IL-1β expression in tumor sections assessed by immunohistochemical staining. The upper images showed the general view of the tumor sections. Bar = 100 μm. The lower images showed the magnified views at 25× magnification. Bar = 20 μm. Data are presented as means ± SEM, with statistical analyses conducted using

induce DNA damage through the oxidation of nucleoside bases [29]. In contrast to nuclear DNA (nDNA), which is protected by histones, mtDNA is more susceptible to ROS-induced damage [30]. To further evaluate oxidative damage, we measured 8-OHdG, a well-established biomarker of ROS-induced DNA damage [31]. As shown in Figure 5D, the 8-OHdG levels in tumor cells increased from 11.64% to 36.65% following radiation exposure. Moreover, immunofluorescence staining demonstrated the colocalization of mitochondria and 8-OHdG in irradiated tumor cells (Figure 5E), indicating that mtDNA is the primary target of ROS rather than nDNA. Collectively, these findings suggest that radiation not only induces apoptosis in tumor cells but also triggers oxidative damage to mtDNA. To investigate whether irradiated tumor cells could promote DCs maturation, non-irradiated and irradiated tumor cells were cocultured with BMDCs for 48 h. FCM analysis showed that the expression of maturation markers CD40 and CD80 on DCs were elevated following irradiated tumor cells stimulation (Supplementary Figure S5D).

To evaluate the direct stimulatory effect of ox-mtDNA on DCs maturation, we isolated mtDNA from irradiated tumor cells in vitro and transfected it into BMDCs using Lipofectamine™ 3000 at a concentration of 5 μg/mL. After 48 h of incubation, we assessed DCs maturation through FCM and measured cytokine levels in the supernatants. As illustrated in Supplementary Figure S5E, the isolated ox-mtDNA significantly enhanced DCs maturation, indicated by increased expression of CD40, CD80, CD86, and MHC II compared to the blank-lipo group. Moreover, the secretion of cytokines such as TNF-α, IL-6, and IL-1β was markedly elevated in the ox-mtDNA group (Figure 5F and Supplementary Figure S5F). Previous studies have reported that ox-mtDNA activates the NLRP3 inflammasome [32, 33]. The activation of the NLRP3 inflammasome leads to its interaction with apoptosis-associated speck-like protein, which facilitates the autocatalytic activation of caspase-1. This activation subsequently cleaves pro-IL-1β, resulting in the production of mature IL-1β [34]. Additionally, AIM2 contributes to inflammasome formation and activation [35]. We observed that ox-mtDNA significantly increased the mRNA levels of *Il-1β* and *Il-18* in DCs (Supplementary Figure S5G). To evaluate the impact of ox-mtDNA on inflammasome activation, we cocultured BMDCs from WT, *Nlrp3*$^{-/-}$ and *Casp1*$^{-/-}$ mice with 5 μg/mL ox-mtDNA, after priming with LPS (500 ng/mL) for 3 h. Following 4 h incubation, we assessed mature IL-1β levels using CBA and concentrated proteins from the culture supernatants for immunoblotting. As illustrated in Figure 5G, IL-1β levels were significantly elevated in WT BMDCs after ox-mtDNA stimulation, whereas production was impaired in *Casp1*$^{-/-}$ BMDCs. A partial reduction in IL-1β production was observed in *Nlrp3*$^{-/-}$ BMDCs, suggesting that ox-mtDNA may activate inflammasomes other than NLRP3, such as the AIM2 inflammasome. Immunoblot analysis of caspase-1 p20 in the supernatants confirmed the secretion levels of IL-1β (Figure 5H). Additionally, immunofluorescence staining demonstrated that ox-mtDNA induced caspase-1 activation in BMDCs derived from WT mice (Figure 5I). Collectively, these findings suggest that ox-mtDNA can activate inflammasome pathway in DCs. Next, we investigated whether 1V209-Cho-Lip, a TLR7 agonist, could activate the NF-κB pathway. BMDCs were stimulated with 1V209-Cho-Lip (5 μg/mL or 10 μg/mL) for 2 h and 6 h. As shown in Figure 5J, we observed an increase in p65 phosphorylation without any change in total p65 protein levels. In contrast, phosphorylated IκBα levels decreased after 2 h due to its degradation by the ubiquitin-proteasome system [36]. In conclusion, 1V209-Cho-Lip activates the NF-κB pathway, which is essential for the expression of pro-IL-1β and NLRP3. Moreover, ox-mtDNA from irradiated tumor cells synergizes with 1V209-Cho-Lip to enhance IL-1β production and promote the maturation of DCs, highlighting their combined potential in antitumor immunity.

3.6 | The antitumor efficacy of RT + 1V209-Cho-Lip was compromised in *Il-1β*$^{-/-}$ and *Casp1*$^{-/-}$ mice

We next investigated the antitumor effect of RT combined with 1V209-Cho-Lip in *Il-1β*$^{-/-}$ and *Casp1*$^{-/-}$ mice, based on our previous findings that 1V209-Cho-Lip serves as the primary signal and ox-mtDNA from irradiated tumor cells acts as the secondary signal to activate the inflammasome pathway in DCs. As anticipated, the combined antitumor effect of 1V209-Cho-Lip and RT was significantly diminished in *Il-1β*$^{-/-}$ and *Casp1*$^{-/-}$ mice. In contrast, tumors in both WT and knockout mice showed similar growth patterns when left untreated (Figure 6A-B). We subsequently examined the immune response in both the tumors and tumor-draining LNs. Consistent with the reduced tumor size, the proportions of activated CD4$^+$ T cells (CD3$^+$CD4$^+$CD69$^+$) and CD8$^+$ T cells (CD3$^+$CD8$^+$CD69$^+$) were lower in tumors from treated

one-way ANOVA. *$P < 0.05$; ***$P < 0.001$. Abbreviations: BMDC, bone marrow-derived dendritic cell; casp1, cysteinyl aspartate specific proteinase 1; CBA, cytometric bead array; GO, gene ontology; IL, interleukin; mRNA, messenger RNA; Nlrp3, NLR family pyrin domain containing 3; R-TCM, irradiated tumor conditioned medium; WT, wild type.

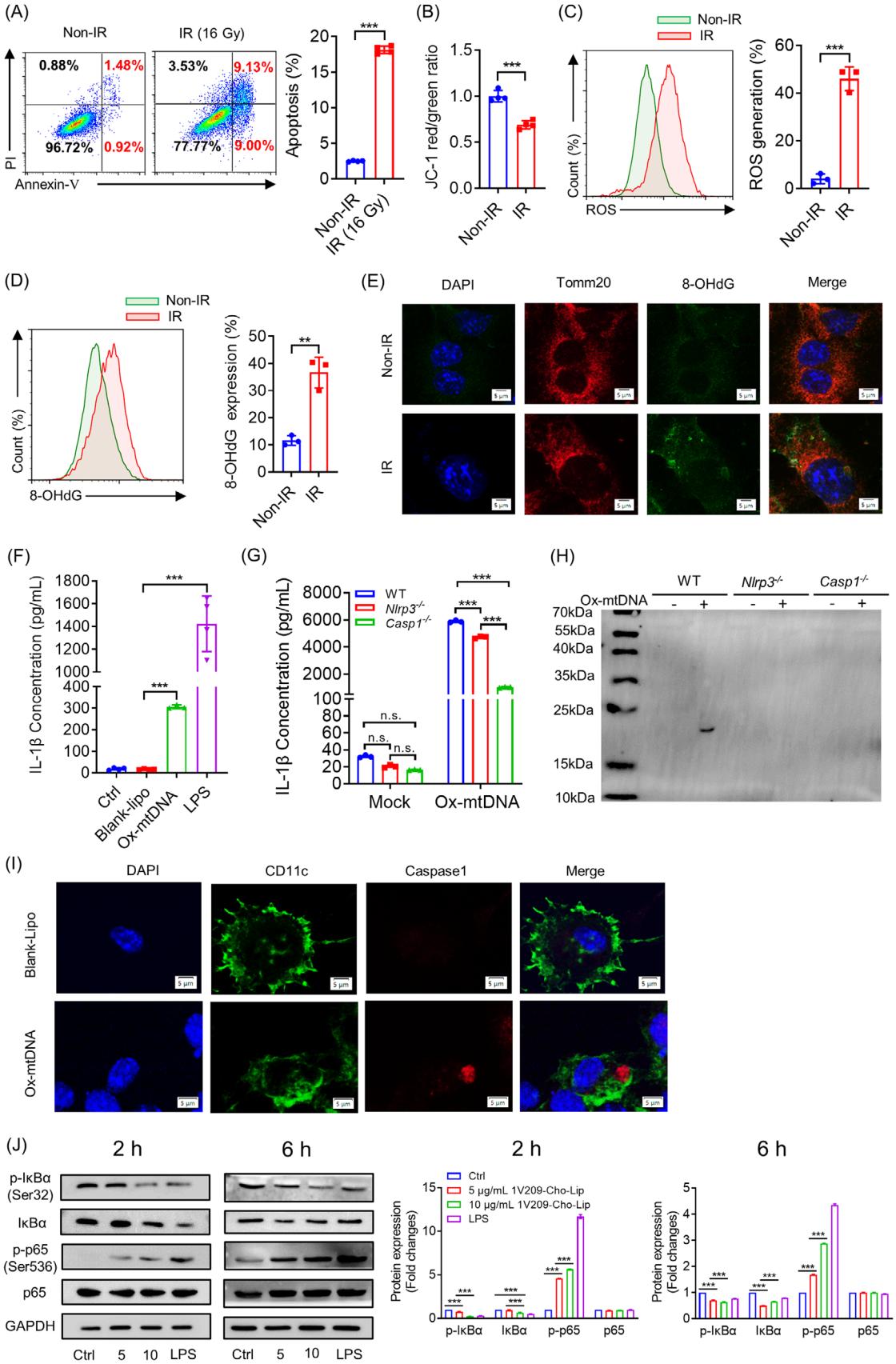

FIGURE 5 Ox-mtDNA from irradiated tumor cells synergized with 1V209-Cho-Lip to activate the inflammasome pathway in DCs. (A) Tumor cells were treated with 16 Gy radiation and then cultured in medium for 48 h. The percentages of apoptotic cells were detected by FCM after Annexin V/PI staining. Representative scatterplots of apoptotic tumor cells were shown in the left panel and quantified in the right

Casp1$^{-/-}$ mice compared to those from treated WT mice (Figure 6C-D). Additionally, the expression of the DCs costimulatory molecules CD80 and CD86 in the tumor-draining LNs of treated *Casp1*$^{-/-}$ mice was also lower than that in treated WT mice (Figure 6E). Taken together, these findings indicate that the inflammasome pathway is crucial for the antitumor immune response elicited by the combined therapy of RT and 1V209-Cho-Lip.

We further evaluated the safety of 1V209-Cho-Lip combined with RT in 4T1 tumor model. No significant changes in body weight were observed (Supplementary Figure S6A). H&E staining showed no notable damage or abnormalities in the tissues of the major organs, suggesting that the treatment was well-tolerated and did not negatively impact organ function or structure (Supplementary Figure S6B). Moreover, serum biochemical analysis of mice from the combined therapy group revealed no significant abnormalities (Supplementary Figure S7). These findings underscore the favorable safety profile of the combined therapy in this study. Mechanistically, 1V209-Cho-Lip activates the NF-κB signaling pathway, promoting the expression of pro-IL-1β. Additionally, Ox-mtDNA released from irradiated tumor cells synergistically activates the inflammasome pathway in DCs, leading to IL-1β production and subsequent DCs maturation. This, in turn, stimulates T cell-mediated immune responses, amplifying the antitumor effect of the combined therapy (Figure 6F).

4 | DISCUSSION

In this study, we demonstrated that 1V209-Cho-Lip combined with RT inhibited tumor growth and enhanced antitumor immunity through activation of the inflammasome-IL-1β pathway. This conclusion is supported by the following findings: (1) the combination therapy inhibited tumor progression and prolonged survival in both 4T1 and B16-F10 tumor models; (2) 1V209-Cho-Lip in combination with R-TCM could enhance maturation, antigen presentation and IL-1β secretion of DCs, further activating T cells to exert antitumor effects; (3) radiation induced apoptosis in tumor cells and triggered oxidative damage to mtDNA, generating oxidized mtDNA as a DAMP; (4) ox-mtDNA synergized with 1V209-Cho-Lip to activate the inflammasome pathway in DCs; (5) the antitumor efficacy of 1V209-Cho-Lip combined with RT was diminished in *Il-1β*$^{-/-}$ and *Casp1*$^{-/-}$ mice. In summary, our results elucidate the mechanisms by which 1V209-Cho-Lip and RT synergize to enhance antitumor immunity via inflammasome-IL-1β activation in DCs, highlighting the potential therapeutic efficacy of this combination strategy for cancer treatment.

Previous studies have reported synergistic effects when TLR7 agonists are combined with RT. A recent investigation demonstrated that systemic administration of the TLR7/8 agonist R848 significantly enhanced the antitumor response induced by stereotactic body RT in murine models of pancreatic cancer, primarily by modifying the tumor immune microenvironment [37]. In mouse models of T and B cell lymphomas, the combination of R848 with RT resulted in long-lasting tumor clearance by promoting the expansion of tumor antigen-specific CD8$^+$ T cells [6]. However, the primary concern with TLR7 agonists is their potential to cause immune-related toxicities, due to the broad expression of TLR7 on immune cells and various normal tissues. For example, sustained

panel (n = 4 per group). (B) MMP in non-IR and IR tumor cells was assessed by FCM using JC-1 staining (n = 4 per group). (C) ROS generation was significantly elevated in IR tumor cells compared to non-IR cells, as indicated by FCM histograms and quantification (n = 3 per group). (D) Representative histograms of FCM and quantification of 8-OHdG expression, a marker of oxidative mtDNA damage, in non-IR and IR tumor cells (n = 3 per group). (E) Immunofluorescence staining was performed using anti-8-OHdG antibody (green), Tomm20 (red), and DAPI (blue, for cell nuclei) in non-IR and IR tumor cells, indicating that mtDNA is the primary target of radiation-induced ROS. Bar = 5 μm. (F) BMDCs were stimulated with ox-mtDNA isolated from irradiated tumor cells, and IL-1β secretion in the supernatants was measured by CBA. LPS was used as positive control (n = 3-4 per group). (G) BMDCs from WT, *Nlrp3*$^{-/-}$, and *Casp1*$^{-/-}$ mice were stimulated with 5 μg/mL ox-mtDNA for 4 h following priming with LPS (500 ng/mL). The supernatants were then collected and analyzed for IL-1β levels using CBA (n = 3 per group). (H) BMDCs from WT, *Nlrp3*$^{-/-}$, and *Casp1*$^{-/-}$ mice were stimulated with 5 μg/mL ox-mtDNA for 4 h following priming with LPS (500 ng/mL). The expression of caspase-1 p20 in the supernatants was detected by immunoblotting after concentration. (I) Immunofluorescence staining was performed for caspase-1 (red), CD11c (green), and DAPI (blue, for cell nuclei) in DCs stimulated with 5 μg/mL ox-mtDNA for 24 h. Bar = 5 μm. (J) BMDCs were stimulated with 1V209-Cho-Lip (5 μg/mL or 10 μg/mL) for 2 h and 6 h. The expression levels of GAPDH, p65, p-p65, IκBα, and p-IκBα were assessed by immunoblotting, with LPS used as positive control. Data are presented as means ± SEM and were analyzed using two-tailed Student's t-tests (A-D), one-way ANOVA (F and J), and two-way ANOVA (G). $^{**}P < 0.01$; $^{***}P < 0.001$; n.s., not significant. Abbreviations: 8-OHdG, 8-hydroxy-2'-deoxyguanosine; BMDC, bone marrow-derived dendritic cell; casp1, cysteinyl aspartate specific proteinase 1; CBA, cytometric bead array; DC, dendritic cell; FCM, flow cytometry; Gy, gray; IL, interleukin; IR, irradiated; IκBα, inhibitor kappa B alpha; LPS, lipopolysaccharides; MMP, mitochondrial membrane potential; Nlrp3, NLR family pyrin domain containing 3; non-IR, non-irradiated; Ox-mtDNA, oxidized mitochondrial DNA; p-IκBα, phosphorylated IκBα; p-p65, phosphorylated p65; ROS, reactive oxygen species; Tomm20, translocase of outer mitochondrial membrane 20; WT, wild type.

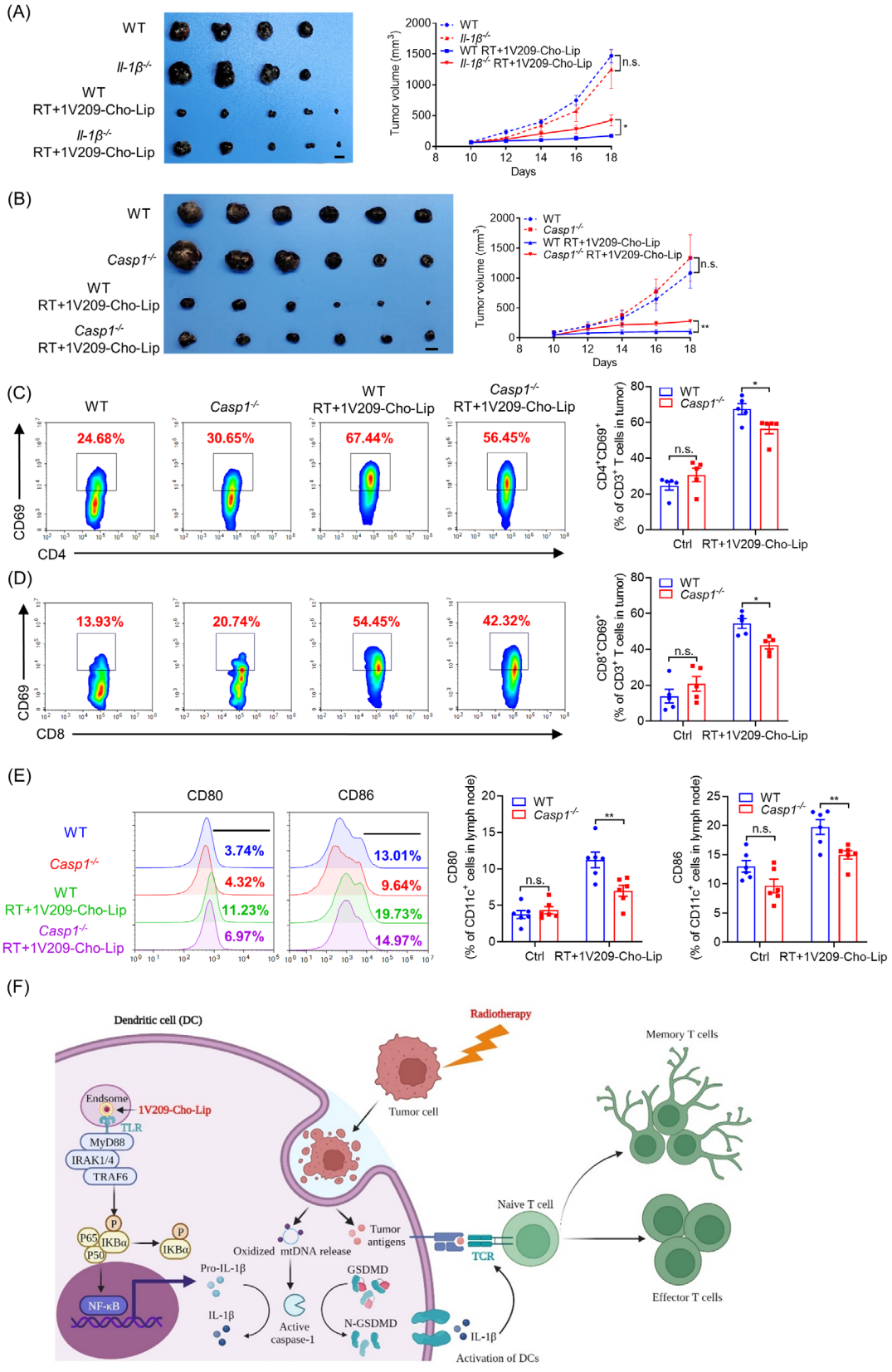

FIGURE 6 The antitumor efficacy of RT + 1V209-Cho-Lip was compromised in *Il-1β*$^{-/-}$ and *Casp1*$^{-/-}$ mice. (A) Images of resected tumors and tumor growth curve for WT and *Il-1β*$^{-/-}$ mice bearing established B16-F10 tumors, with or without combination therapy (n = 4-5 per group). Bar = 10 mm. (B) Images of resected tumors and tumor growth curve for WT and *Casp1*$^{-/-}$ mice bearing established B16-F10 tumors, with or without combination therapy (n = 6 per group). Bar = 10 mm. (C-D) FCM plots and quantification showed significantly lower percentages of activated CD4$^+$ T cells (CD3$^+$CD4$^+$CD69$^+$, C) and CD8$^+$ T cells (CD3$^+$CD8$^+$CD69$^+$, D) in tumors of *Casp1*$^{-/-}$ mice compared

stimulation of TLR7 has been shown to induce lymphopenia, splenomegaly, increased levels of pro-inflammatory cytokines, and a reduction in lymphoid subsets [19]. To address these concerns, our team previously developed cholesterolized TLR7 agonist liposomes, 1V209-Cho-Lip, which demonstrated minimal toxic effects and no severe immune-related adverse events. Despite its favorable safety profile, 1V209-Cho-Lip exhibited limited efficacy when used alone in treating 4T1 subcutaneous tumors [21]. In this study, we treated 4T1 and B16-F10 subcutaneous tumors with a combination of 1V209-Cho-Lip and RT, yielding significant antitumor efficacy and demonstrating a favorable safety profile. Additionally, while the mechanisms underlying the synergy between RT and TLR7 agonists remain poorly understood, our findings provide new insights into the potential mechanisms driving the enhanced antitumor response observed with this combination therapy.

Irradiation-driven immunogenic cell death can result in the exposure or release of various DAMPs, including the translocation of calreticulin (CRT) to the cell surface and the extracellular release of high mobility group box 1 (HMGB1) and adenosine triphosphate (ATP) [38–40]. Additionally, X-rays can induce the generation of endogenous ROS in mitochondria and alter mitochondrial membrane permeability, further amplifying ROS levels [41, 42]. Elevated levels of ROS can lead to the oxidation of DNA bases. Due to the absence of protective histones and repair proteins, mtDNA is particularly vulnerable to ROS-induced damage compared to nuclear DNA [30]. In this study, we observed a significant increase in ROS generation and a reduction in MMP following radiation treatment. Furthermore, the levels of 8-OHdG, a marker of oxidative DNA damage, in irradiated tumor cells were elevated, and this modification was found to colocalize with mitochondria, consistent with previous findings [43]. The isolated ox-mtDNA from irradiated tumor cells was shown to stimulate DCs maturation in vitro. Thus, we propose that ox-mtDNA, acting as DAMPs, plays a pivotal role in activating the antitumor immune response in the RT + 1V209-Cho-Lip treatment group. However, our study does not rule out the potential involvement of other DAMPs, such as ATP, in effectively eliciting antitumor immunity. Indeed, previous research has demonstrated that ATP released from dying tumor cells activates P2X(7) purinergic receptors on DCs, thereby triggering a $CD8^+$ T cell immune response [44].

Our study demonstrated that oxidized mtDNA activates the inflammasome pathway in DCs, resulting in the production of IL-1β. Previous research has underscored the essential role of mitochondria in NLRP3 inflammasome activation [23, 32, 45]. Shimada *et al.* [32] reported that ox-mtDNA released during programmed cell death triggers NLRP3 inflammasome activation. In our experiments, IL-1β production was reduced in *Casp1*$^{-/-}$ and *Nlrp3*$^{-/-}$ BMDCs when cocultured with ox-mtDNA, underscoring the involvement of the NLRP3 inflammasome and caspase-1 in this process. Han *et al.* [46] demonstrated that radiation induced the activation of both AIM2 and NLRP3 inflammasomes. Moreover, tumors transplanted into *Casp1*$^{-/-}$ or *Aim2*$^{-/-}$*Nlrp3*$^{-/-}$ mice showed resistance to radiation treatment, emphasizing the critical role of inflammasome signaling in mediating the antitumor effects of RT. The synergy between ox-mtDNA and 1V209-Cho-Lip in stimulating the inflammasome pathway provides a mechanistic link between radiation-induced cell death and the subsequent activation of the immune system, further amplifying the therapeutic effects of the combination treatment.

However, the study has several limitations. First, our study primarily relies on animal models, and while these models are valuable for understanding mechanisms, they may not fully represent human physiological responses. Second, although the inflammasome-IL-1β pathway is identified as a key mechanism, other potential mechanisms contributing to the antitumor effects of the therapy remain unexplored. The complex interactions between the therapies and other immune cells or signaling pathways are yet to be fully understood. Third, the study does not compare the combination therapy to other standard or emerging treatments. Without such comparisons, it is challenging to determine whether the combination of 1V209-Cho-Lip and RT provides a superior or comparable therapeutic benefit to existing approaches.

5 | CONCLUSIONS

In conclusion, the combination of 1V209-Cho-Lip and RT demonstrated significant antitumor efficacy by activating the inflammasome-IL-1β pathway in DCs. These findings highlight a promising strategy for developing combinatorial therapeutic approaches that leverage both direct tumor cell targeting and immune system activation, thereby

to WT mice following combination therapy ($n = 5$ per group). (E) Representative FCM histograms and quantification of DCs maturation markers in tumor-draining LNs ($n = 6$ per group). (F) Schematic illustration summarizing the mechanism of the antitumor immune response induced by1V209-Cho-Lip in combination with RT. Data are presented as means ± SEM, and analyzed with two-way ANOVA test. *$P < 0.05$; **$P < 0.01$; n.s., not significant. Abbreviations: casp1, cysteinyl aspartate specific proteinase 1; DC, dendritic cell; FCM, flow cytometry; IL, interleukin; LN, lymph node; RT, radiotherapy; WT, wild type.

improving treatment outcomes in cancer patients. Further studies are warranted to explore the clinical relevance of this combination therapy.

AUTHOR CONTRIBUTIONS

Xuejiao Han and Yuquan Wei designed the study and conducted the majority of experiments. The manuscript was written by Xuejiao Han. Dandan Wan was responsible for synthesizing 1V209-Cho-Lip. Yuan Cheng, Aqu Alu, and Ziqi Zhang performed the experiments. Zhenfei Bi, Manni Wang, Yan Tang, and Weiqi Hong analyzed the data. Siyuan Chen and Li Chen prepared the figures. Yuquan Wei revised this manuscript and supervised the research. All authors reviewed and approved the final version of the manuscript.

ACKNOWLEDGEMENTS

We would like to express our gratitude to the colleagues from our research group for their invaluable assistance. This work was supported by the National Science Foundation for Excellent Young Scholars (32122052), National Natural Science Foundation Regional Innovation and Development (No. U19A2003), National Natural Science Foundation of China (82102896), China Postdoctoral Science Foundation (2024M762248), Natural Science Foundation of Sichuan Province (2024NSFSC1883), and Postdoctor Research Fund of West China Hospital, Sichuan University (2024HXBH055).

CONFLICT OF INTEREST STATEMENT

The authors declare that they have no competing interests.

DATA AVAILABILITY STATEMENT

The data that support the findings of this study are available from the corresponding author upon reasonable request.

ETHICS APPROVAL AND CONSENT TO PARTICIPATE

Animal experiments were approved by the State Key Laboratory of Biotherapy Animal Care and Use Committee of Sichuan University, China (20250108003).

ORCID

Xuejiao Han https://orcid.org/0000-0002-9842-8990

REFERENCES

1. Thariat J, Hannoun-Levi JM, Sun Myint A, Vuong T, Gérard JP. Past, present, and future of radiotherapy for the benefit of patients. Nat Rev Clin Oncol. 2013;10(1):52-60.
2. Kono H, Rock KL. How dying cells alert the immune system to danger. Nat Rev Immunol. 2008;8(4):279-89.
3. Golden EB, Apetoh L. Radiotherapy and immunogenic cell death. Semin Radiat Oncol. 2015;25(1):11-7.
4. Wu Y, Yi M, Niu M, Zhou B, Mei Q, Wu K. Beyond success: unveiling the hidden potential of radiotherapy and immunotherapy in solid tumors. Cancer Commun (Lond). 2024;44(7):739-60.
5. Demaria S, Ng B, Devitt ML, Babb JS, Kawashima N, Liebes L, et al. Ionizing radiation inhibition of distant untreated tumors (abscopal effect) is immune mediated. Int J Radiat Oncol Biol Phys. 2004;58(3):862-70.
6. Dovedi SJ, Melis MH, Wilkinson RW, Adlard AL, Stratford IJ, Honeychurch J, et al. Systemic delivery of a TLR7 agonist in combination with radiation primes durable antitumor immune responses in mouse models of lymphoma. Blood. 2013;121(2):251-9.
7. Castro F, Pinto ML, Pereira CL, Serre K, Barbosa MA, Vermaelen K, et al. Chitosan/γ-PGA nanoparticles-based immunotherapy as adjuvant to radiotherapy in breast cancer. Biomaterials. 2020;257:120218.
8. Formenti SC, Rudqvist NP, Golden E, Cooper B, Wennerberg E, Lhuillier C, et al. Radiotherapy induces responses of lung cancer to CTLA-4 blockade. Nat Med. 2018;24(12):1845-51.
9. Voorwerk L, Slagter M, Horlings HM, Sikorska K, van de Vijver KK, de Maaker M, et al. Immune induction strategies in metastatic triple-negative breast cancer to enhance the sensitivity to PD-1 blockade: the TONIC trial. Nat Med. 2019;25(6):920-8.
10. Shao C, Zhang Y, Li H, Chen J, Huang T, Li J, et al. Radiotherapy-resistant prostate cancer cells escape immune checkpoint blockade through the senescence-related ataxia telangiectasia and Rad3-related protein. Cancer Commun (Lond). 2024.
11. Kawai T, Ikegawa M, Ori D, Akira S. Decoding Toll-like receptors: Recent insights and perspectives in innate immunity. Immunity. 2024;57(4):649-73.
12. Bekeredjian-Ding I, Jego G. Toll-like receptors–sentries in the B-cell response. Immunology. 2009;128(3):311-23.
13. Girart MV, Fuertes MB, Domaica CI, Rossi LE, Zwirner NW. Engagement of TLR3, TLR7, and NKG2D regulate IFN-gamma secretion but not NKG2D-mediated cytotoxicity by human NK cells stimulated with suboptimal doses of IL-12. J Immunol. 2007;179(6):3472-9.
14. Walshaw RC, Honeychurch J, Choudhury A, Illidge TM. Toll-Like Receptor Agonists and Radiation Therapy Combinations: An Untapped Opportunity to Induce Anticancer Immunity and Improve Tumor control. Int J Radiat Oncol Biol Phys. 2020;108(1):27-37.
15. Latz E, Verma A, Visintin A, Gong M, Sirois CM, Klein DC, et al. Ligand-induced conformational changes allosterically activate Toll-like receptor 9. Nat Immunol. 2007;8(7):772-9.
16. Frank MJ, Reagan PM, Bartlett NL, Gordon LI, Friedberg JW, Czerwinski DK, et al. In Situ Vaccination with a TLR9 Agonist and Local Low-Dose Radiation Induces Systemic Responses in Untreated Indolent Lymphoma. Cancer Discov. 2018;8(10):1258-69.
17. Lee J, Chuang TH, Redecke V, She L, Pitha PM, Carson DA, et al. Molecular basis for the immunostimulatory activity of guanine nucleoside analogs: activation of Toll-like receptor 7. Proc Natl Acad Sci U S A. 2003;100(11):6646-51.
18. Nishiya T, DeFranco AL. Ligand-regulated chimeric receptor approach reveals distinctive subcellular localization and

signaling properties of the Toll-like receptors. J Biol Chem. 2004;279(18):19008-17.
19. Baenziger S, Heikenwalder M, Johansen P, Schlaepfer E, Hofer U, Miller RC, et al. Triggering TLR7 in mice induces immune activation and lymphoid system disruption, resembling HIV-mediated pathology. Blood. 2009;113(2):377-88.
20. Schön MP, Schön M. TLR7 and TLR8 as targets in cancer therapy. Oncogene. 2008;27(2):190-9.
21. Wan D, Que H, Chen L, Lan T, Hong W, He C, et al. Lymph-Node-Targeted Cholesterolized TLR7 Agonist Liposomes Provoke a Safe and Durable Antitumor Response. Nano Lett. 2021;21(19):7960-9.
22. Zhang Z, Yuan B, Bao M, Lu N, Kim T, Liu YJ. The helicase DDX41 senses intracellular DNA mediated by the adaptor STING in dendritic cells. Nat Immunol. 2011;12(10):959-65.
23. Nakahira K, Haspel JA, Rathinam VA, Lee SJ, Dolinay T, Lam HC, et al. Autophagy proteins regulate innate immune responses by inhibiting the release of mitochondrial DNA mediated by the NALP3 inflammasome. Nat Immunol. 2011;12(3):222-30.
24. Wu X, Xiong E, Wang W, Scali M, Cresti M. Universal sample preparation method integrating trichloroacetic acid/acetone precipitation with phenol extraction for crop proteomic analysis. Nat Protoc. 2014;9(2):362-74.
25. Vanpouille-Box C, Alard A, Aryankalayil MJ, Sarfraz Y, Diamond JM, Schneider RJ, et al. DNA exonuclease Trex1 regulates radiotherapy-induced tumour immunogenicity. Nat Commun. 2017;8:15618.
26. Zhang Z, Li X, Wang Y, Wei Y, Wei X. Involvement of inflammasomes in tumor microenvironment and tumor therapies. J Hematol Oncol. 2023;16(1):24.
27. Fucikova J, Kepp O, Kasikova L, Petroni G, Yamazaki T, Liu P, et al. Detection of immunogenic cell death and its relevance for cancer therapy. Cell Death Dis. 2020;11(11):1013.
28. Wei X, Shao B, He Z, Ye T, Luo M, Sang Y, et al. Cationic nanocarriers induce cell necrosis through impairment of Na(+)/K(+)-ATPase and cause subsequent inflammatory response. Cell Res. 2015;25(2):237-53.
29. Srinivas US, Tan BWQ, Vellayappan BA, Jeyasekharan AD. ROS and the DNA damage response in cancer. Redox Biol. 2019;25:101084.
30. Sabharwal SS, Schumacker PT. Mitochondrial ROS in cancer: initiators, amplifiers or an Achilles' heel? Nat Rev Cancer. 2014;14(11):709-21.
31. Wiseman H, Halliwell B. Damage to DNA by reactive oxygen and nitrogen species: role in inflammatory disease and progression to cancer. Biochem J. 1996;313(Pt 1):17-29.
32. Shimada K, Crother TR, Karlin J, Dagvadorj J, Chiba N, Chen S, et al. Oxidized mitochondrial DNA activates the NLRP3 inflammasome during apoptosis. Immunity. 2012;36(3):401-14.
33. Xian H, Liu Y, Rundberg Nilsson A, Gatchalian R, Crother TR, Tourtellotte WG, et al. Metformin inhibition of mitochondrial ATP and DNA synthesis abrogates NLRP3 inflammasome activation and pulmonary inflammation. Immunity. 2021;54(7):1463-77.e11.
34. Martinon F, Mayor A, Tschopp J. The inflammasomes: guardians of the body. Annu Rev Immunol. 2009;27:229-65.
35. Guo H, Callaway JB, Ting JP. Inflammasomes: mechanism of action, role in disease, and therapeutics. Nat Med. 2015;21(7):677-87.
36. Takeuchi O, Akira S. Pattern recognition receptors and inflammation. Cell. 2010;140(6):805-20.
37. Ye J, Mills BN, Qin SS, Garrett-Larsen J, Murphy JD, Uccello TP, et al. Toll-like receptor 7/8 agonist R848 alters the immune tumor microenvironment and enhances SBRT-induced antitumor efficacy in murine models of pancreatic cancer. J Immunother Cancer. 2022;10(7):e004784.
38. Panaretakis T, Kepp O, Brockmeier U, Tesniere A, Bjorklund AC, Chapman DC, et al. Mechanisms of pre-apoptotic calreticulin exposure in immunogenic cell death. Embo j. 2009;28(5):578-90.
39. Lotze MT, Tracey KJ. High-mobility group box 1 protein (HMGB1): nuclear weapon in the immune arsenal. Nat Rev Immunol. 2005;5(4):331-42.
40. Golden EB, Frances D, Pellicciotta I, Demaria S, Helen Barcellos-Hoff M, Formenti SC. Radiation fosters dose-dependent and chemotherapy-induced immunogenic cell death. Oncoimmunology. 2014;3:e28518.
41. Leach JK, Van Tuyle G, Lin PS, Schmidt-Ullrich R, Mikkelsen RB. Ionizing radiation-induced, mitochondria-dependent generation of reactive oxygen/nitrogen. Cancer Res. 2001;61(10):3894-901.
42. Tulard A, Hoffschir F, de Boisferon FH, Luccioni C, Bravard A. Persistent oxidative stress after ionizing radiation is involved in inherited radiosensitivity. Free Radic Biol Med. 2003;35(1):68-77.
43. Fang C, Mo F, Liu L, Du J, Luo M, Men K, et al. Oxidized mitochondrial DNA sensing by STING signaling promotes the antitumor effect of an irradiated immunogenic cancer cell vaccine. Cell Mol Immunol. 2021;18(9):2211-23.
44. Ghiringhelli F, Apetoh L, Tesniere A, Aymeric L, Ma Y, Ortiz C, et al. Activation of the NLRP3 inflammasome in dendritic cells induces IL-1beta-dependent adaptive immunity against tumors. Nat Med. 2009;15(10):1170-8.
45. Zhong Z, Liang S, Sanchez-Lopez E, He F, Shalapour S, Lin XJ, et al. New mitochondrial DNA synthesis enables NLRP3 inflammasome activation. Nature. 2018;560(7717):198-203.
46. Han C, Godfrey V, Liu Z, Han Y, Liu L, Peng H, et al. The AIM2 and NLRP3 inflammasomes trigger IL-1-mediated antitumor effects during radiation. Sci Immunol. 2021;6(59):eabc6998.

SUPPORTING INFORMATION

Additional supporting information can be found online in the Supporting Information section at the end of this article.

How to cite this article: Han X, Cheng Y, Wan D, Alu A, Zhang Z, Bi Z, et al. Enhancing antitumor immunity through the combination of cholesterolized TLR7 agonist liposomes and radiotherapy: a role for IL-1β and the inflammasome pathway. Cancer Commun.. 2025;1–19. https://doi.org/10.1002/cac2.70024